Article

A Fast Photoswitch for Minimally Perturbed Peptides: Investigation of the trans → cis Photoisomerization of *N*-Methylthioacetamide

Jan Helbing, Harald Bregy, Jens Bredenbeck, Rolf Pfister, Peter Hamm, Robert Huber, Josef Wachtveitl, Luca De Vico, and Massimo Olivucci

J. Am. Chem. Soc., **2004**, 126 (28), 8823-8834• DOI: 10.1021/ja049227a • Publication Date (Web): 23 June 2004

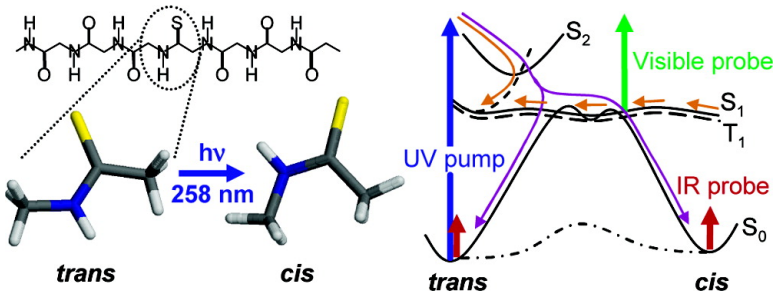

More About This Article

Additional resources and features associated with this article are available within the HTML version:

- Supporting Information
- Links to the 7 articles that cite this article, as of the time of this article download
- Access to high resolution figures
- Links to articles and content related to this article
- Copyright permission to reproduce figures and/or text from this article

View the Full Text HTML

J|A|C|S
ARTICLES
Published on Web 06/23/2004

A Fast Photoswitch for Minimally Perturbed Peptides: Investigation of the trans → cis Photoisomerization of *N*-Methylthioacetamide

Jan Helbing,[†] Harald Bregy,[†] Jens Bredenbeck,[†] Rolf Pfister,[†] Peter Hamm,*[,†] Robert Huber,[‡] Josef Wachtveitl,[‡] Luca De Vico,[§] and Massimo Olivucci*[,§,||]

Contribution from the Physikalisch-Chemisches Institut, Winterthurerstrasse 190, Universität Zürich, CH-8057 Zürich, Switzerland, Institut für Physikalische und Theoretische Chemie, Johann Wolfgang Goethe - Universität, Frankfurt am Main, Germany, Dipartimento di Chimica, Università degli Studi di Siena, Via Aldo Moro, 53100 Siena, Italy, and Centro per lo Studio dei Sistemi Complessi, Via Tommaso Pendola 37, 53100 Siena, Italy

Received February 12, 2004; E-mail: phamm@pci.unizh.ch; olivucci@unisi.it

Abstract: Thio amino acids can be integrated into the backbone of peptides without significantly perturbing their structure. In this contribution we use ultrafast infrared and visible spectroscopy as well as state-of-the-art ab initio computations to investigate the photoisomerization of the trans form of *N*-methylthioacetamide (NMTAA) as a model conformational photoswitch. Following the S_2 excitation of *trans*-NMTAA in water, the return of the molecule into the trans ground state and the formation of the cis isomer is observed on a dual time scale, with a fast component of 8−9 ps and a slow time constant of ∼250 ps. On both time scales the probability of isomerization to the cis form is found to be 30−40%, independently of excitation wavelength. Ab initio CASPT2//CASSCF photochemical reaction path calculations indicate that, in vacuo, the trans → cis isomerization event takes place on the S_1 and/or T_1 triplet potential energy surfaces and is controlled by very small energy barriers, in agreement with the experimentally observed picosecond time scale. Furthermore, the calculations identify one S_2/S_1 and four nearly isoenergetic S_1/S_0 conical intersection decay channels. In line with the observed isomerization probability, only one of the S_1/S_0 conical intersections yields the cis conformation upon $S_1 \rightarrow S_0$ decay. A substantially equivalent excited-state relaxation results from four T_1/S_0 intersystem crossing points.

1. Introduction

While amides are usually most stable in the trans conformation, they can be converted into the cis conformation with relatively high quantum yield by photoisomerization upon $\pi-\pi^*$ excitation.[1] In *N*-methylacetamide (NMA) the corresponding absorption band peaks at 186 nm.[2] Substitution of oxygen by sulfur in a peptide bond yields a thioamide and leads to significantly red-shifted $\pi-\pi^*$ and $n-\pi^*$ absorption, thus lowering the excitation energy needed for photoisomerization. When a thioamide is integrated into the backbone of a polypeptide, it is therefore possible to selectively excite this unit and to photoinduce a conformational change via trans−cis isomerization at a well-defined position in the peptide chain. For the thionated endorphins Tyr-ϕ[CS-N]-Pro-X-Phe-NH_2 (X = Trp or Phe) Schutkowski and co-workers have shown that the concentration of molecules with the Tyr-Pro bond in the cis conformation can be significantly enhanced by photoisomerization.[3] Seebach and co-workers[4] have synthesized β-thiohexapeptides with one, two, and three C═S groups in the N-terminal position and report drastic changes in the CD-spectra upon $\pi-\pi^*$ excitation of the thionated peptide units. In very recent work, Zhao et al. report on efficient photoswitching of secondary thiopeptide bonds in α-polypeptides.[5] This is particularly interesting as the possibility to selectively introduce thio amino acids into polypeptides, which are capable of forming secondary structures, has recently been demonstrated by Miwa and co-workers.[6,7] The incorporation of a thioamide linkage both between the residues of a β-turn[6] and within a helical peptide[7] resulted only in minor changes to the native hairpin and α-helical structures. As an alternative to the more widely used, but much bulkier azobenzene photoswitches,[8−10] O → S substitution in a single peptide unit may thus provide a method to study the

[†] Physikalisch-Chemisches Institut, Winterthurerstrasse 190, Universität Zürich, CH-8057 Zürich, Switzerland.
[‡] Institut für Physikalische und Theoretische Chemie, Johann Wolfgang Goethe − Universität Frankfurt am Main, Germany.
[§] Dipartimento di Chimica, Università degli Studi di Siena, Via Aldo Moro, 53100 Siena, Italy.
[||] Centro per lo Studio dei Sistemi Complessi, Via Tommaso Pendola 37, 53100 Siena, Italy.

(1) Song, S.; Asher, S. A.; Krimm, S.; Shaw, K. D. *J. Am. Chem. Soc.* **1991**, *113*, 1155.
(2) Nielsen, E. B.; Schellman, J. A. *J. Phys. Chem.* **1967**, *71*, 2297.
(3) Frank, R.; Jakob, M.; Thunecke, F.; Fischer, G.; Schutkowski, M. *Angew. Chem., Int. Ed.* **2000**, *39*, 1120.
(4) Sifferlen, T.; Rueping, M.; Gademann, K.; Jaun, B.; Seebach, D. *Helv. Chim. Acta* **1999**, *82*, 2067.
(5) Zhao, J.; Wildemann, D.; Jakob, M.; Vargas, C.; Schiene-Fischer, C. *Chem. Commun.* **2003**, 2810.
(6) Miwa, J. H.; Patel, A. K.; Vivatrat, N.; Popek, S. M.; Meyer, A. M. *Org. Lett.* **2001**, *3*, 3373.
(7) Miwa, J. H.; Pallivathucal, L.; Gowda, S.; Lee, K. E. *Org. Lett.* **2002**, *4*, 4655.

dynamics of photoinduced conformational changes in practically *unperturbed* (i.e., substantially native) peptides and proteins, provided that isomerization of the thioamide takes place on a sufficiently fast time scale.

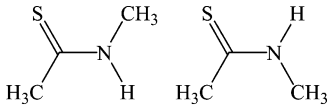

trans-NMTAA *cis*-NMTAA

N-Methylthioacetamide (NMTAA) is among the simplest thioamides, and it has been subject to many studies of photoisomerization, using UV−vis, Raman, and NMR spectroscopy.[11−13] It has been shown that trans−cis isomerization[14] leads to significant shifts in both the electronic and the vibrational spectra, which in turn can be used to monitor the kinetics and dynamics of photoisomerization. However, these experiments, as well as similar measurements on regular amides,[1,15] provide only limited information on the underlying mechanism and the time scales involved. The best time resolution thus far was achieved by resonance Raman experiments, which have put a 5-ns upper limit for the time of trans → cis isomerization of NMTAA.[12] While the high isomerization efficiency upon UV excitation has been interpreted as a signature of a twisted $\pi-\pi^*$ excited state in NMA and NMTAA,[1] torsional modes are not enhanced in the resonance Raman spectra of NMA,[15] indicating that isomerization may occur later in the relaxation process. Early ab initio calculations[16] have reported optimized structures with twisted geometry in both the $n-\pi^*$, $\pi-\pi^*$ and the triplet excited states of NMA.

Here, to establish the photoisomerization mechanism of NMTAA, we have used transient visible and infrared spectroscopy with high time resolution to follow the photoreaction in real time. In addition we have performed kinetic measurements of the isomerization quantum yields and photostabilities at different irradiation wavelengths. To provide a rigorous basis for the formulation of a mechanism consistent with the observed results we have performed ab initio CASPT2//CASSCF quantum chemical calculations to map out the intrinsic (i.e., in vacuo) photoisomerization path of NMTAA.

2. Methods

2.1. Experimental Setup. NMTAA was prepared from NMA, employing standard procedures based on Lawesson's reagent[17] and purified by vacuum distillation. For time-resolved IR measurements, 50−250 mM solutions of NMTAA in D_2O were circulated through a flow cell made of CaF_2 windows spaced 50 μm apart at a rate sufficient to ensure complete exchange of excited sample volume between subsequent excitation pulses.[18]

To completely avoid signals from the window material in measurements in the visible spectral range, experiments had to be performed in a jet of NMTAA, dissolved in doubly distilled water, with a thickness of about 70 μm. A high optical density of the NMTAA solution of about 100 OD/mm ($c \approx 80$ mM) provided a low effective interaction path length between pump light and the water to further minimize contributions from the solvent.

Femtosecond (fs) pulses for IR measurements (1 kHz, 700 μJ /pulse, 80 fs) were obtained from an amplified titanium/sapphire laser system (Spectra Physics), operating either at 840 or at 777 nm. UV pulses for the excitation of NMTAA at 280 or at 259 nm were generated by frequency tripling. The third harmonic beam was then isolated by dielectric mirrors, and the UV pulses were stretched to 1.4 ps duration by guiding them through 15 cm of fused silica. This significantly increased the threshold for the onset of undesired nonlinear effects in the sample cell, such as white-light generation and/or color center formation, and allowed excitation of a larger fraction of the molecules.

Mid-infrared pulses near 1400 cm^{-1} (100 fs, 1 μJ, 250 cm^{-1} bandwidth) were produced in a home-built double-stage optical parametric amplifier (OPA) followed by frequency mixing in a $AgGaS_2$ (silver thiogallate) crystal.[19] The IR pulses were split into two parts (of ~50 nJ each). One part (the probe pulse) was overlapped with the UV-pump pulse in the sample cell. The second part was used as a reference beam to correct for intensity fluctuations and crossed the flow-cell approximately 500 μm further upstream than the pump pulse. Both IR beams were dispersed in a spectrometer and detected with a double MCT array (2 × 32 pixels) on a single-shot basis with 3 cm^{-1} resolution.

For transient UV-pump/vis-probe spectroscopy a Clark MRX CPA-2001 regenerative amplifier system (1 kHz, 800 μJ /pulse, 160 fs) provided pulses with a central wavelength of 775 nm, and frequency tripling yielded UV pulses at 258 nm. The pulse energies for excitation were chosen low (between 300 nJ and 2 μJ) to minimize the formation of solvated electrons by multiphoton excitation. Transient absorbance changes in the UV−visible spectral range were recorded by a single-filament white-light continuum, generated in a 2-mm-thick CaF_2 plate, which covered a wavelength range from 300 to 1000 nm. For spectral resolution two spectrometers (for probe and reference beams) equipped with 42-diode arrays were used and operated in single-shot detection.

Narrow bandwidth light for kinetic measurements was generated by passing the output of a high-pressure Xe lamp through a monochromator. The UV light was directed onto the sample, either inside an FTIR or a UV−vis spectrometer, allowing recording of spectra as a function of irradiation without having to move the sample. A flow cell allowed introduction or exchange of the sample in the FTIR spectrometer, without opening the thermally equilibrated and nitrogen-flushed chamber, and guaranteed identical optical path lengths, window absorption, and scattering conditions in all experiments. All data were recorded with a liquid nitrogen-cooled MCT detector, and baseline drifts were less than 1 mOD over several hours. Care was taken that the spot size used for irradiation was larger than the sample cell window. The photon flux could thus be determined from a measurement of the light power immediately behind an empty sample cell. The same excitation source was used for fluorescence measurements in combination with a photomultiplier and a photon counting system. A lower limit for the sensitivity of this home-built setup was determined from the fluorescence signal of a laser dye of identical optical density at the excitation wavelength.

^{1}H NMR spectra in thermal equilibrium and of the photostationary state were recorded with an Avance DRX-600 MHz spectrometer. To ensure full saturation of the large amount of sample needed, we

(8) Behrendt, R.; Renner, C.; Schenk, M.; Wang, F.; Wachtveitl, J.; Oesterhelt, D.; Moroder, L. *Angew. Chem., Int. Ed.* **1999**, *38*, 2771.
(9) Renner, C.; Behrendt, R.; Spörlein, S.; Wachtveitl, J.; Moroder, L. *Biopolymers* **2000**, *54*, 489.
(10) Kumita, J. R.; Smart, O. S.; Woolley, G. A. *Proc. Natl. Acad. Sci. U.S.A.* **2000**, *97*, 3803.
(11) Harada, I.; Tasumi, M. *Chem. Phys. Lett.* **1980**, *70*, 279.
(12) Kato, C.; Hamaguchi, H.; Tasumi, M. *J. Phys. Chem.* **1985**, *89*, 407.
(13) Frank, R.; Jakob, M.; Thunecke, F.; Fischer, G.; Schutkowski, M. *J. Phys. Chem. A* **2000**, *104*, 7957.
(14) Since the isomerization takes place about the formally single bond C−N, one should refer to *s-trans*-NMTAA and *s-cis*-NMTAA conformations. However, to conform to previous works, we use the labels cis or trans determined by the relative positions of the two NMTAA methyl groups.
(15) Chen, X. G.; Asher, S. A.; Schweitzer-Stenner, R.; Mirkin, N. G.; Krimm, S. *J. Am. Chem. Soc.* **1995**, *117*, 2884.
(16) Li, Y.; Garrell, R. L.; Houk, K. N. *J. Am. Chem. Soc.* **1991**, *113*, 5895.
(17) Thomsen, I.; Clausen, K.; Scheibye, S.; Lawesson, S.-O. *Org. Synth.* **1984**, *62*, 158.
(18) Bredenbeck, J.; Hamm, P. *Rev. Sci. Instrum.* **2003**, *74*, 3188.
(19) Hamm, P.; Kaindl, R. A.; Stenger, J. *Opt. Lett.* **2000**, *25*, 1798.

irradiated with 3−6 mW UV light from the fs-laser, while circulating the sample inside the flow cell and monitoring its UV-absorption spectrum. The saturated sample was then transferred to the NMR spectrometer, and spectra were recorded within 10 min after the end of irradiation.

2.2. Computational Methods. Structure optimization and relaxation path mapping have been carried out using fully unconstrained ab initio quantum chemical computations in the framework of the CASPT2//CASSCF strategy, with the only exception of two triplet energy minima (**Min T_1 Planar Trans** and **Min T_1 Planar Cis**) that were optimized by imposing a planarity constraint.[20,21] Relaxation paths were computed in terms of minimum energy path (MEP) in mass-weighted coordinates, using the IRD methodology.[22,23] The CASPT2//CASSCF strategy requires that the reaction coordinate is computed at the complete active space self-consistent field (CASSCF) level and that the corresponding energy profile is reevaluated on the multiconfigurational second-order Møller−Plesset perturbation theory level (here we used the CASPT2 method[24] implemented in MOLCAS-5)[25] to take into account the effect of electron dynamic correlation.

All computations employed the 6-31G* basis set and an active space comprising 10 electrons in 8 orbitals. This includes the full N−C−S π-system (4 electrons in 3 π-orbitals), the sulfur p lone pair (2 electrons in 1 orbital), plus the C−N and C−S bonds (4 electrons in 4 σ-orbitals). The σ/σ^* orbitals were added after test calculations because they were seen to mix with the π/π^* and lone pair systems when the geometry becomes highly pyramidalized. All geometry optimizations were carried out using the GAUSSIAN98 suite of programs.[26]

When possible, energy minima and transition structures were optimized using a single root CASSCF wave function and confirmed via analytic frequency computations. However, the S_2 minimum (**Min S_2**) was located using a two-root (S_1,S_2) state-average (0.5,0.5) CASSCF wave function and was subsequently confirmed via a numerical frequency calculation. Similarly, due to wave function instability, the four S_0 transition states (**TS S_0 A1**, **TS S_0 A2**, **TS S_0 B1**, **TS S_0 B2**) were located using a two roots (S_0,S_1) state-average (0.5,0.5) CASSCF wave function.

The S_2, S_1, T_2, T_1, and S_0 potential energy surfaces were connected by computing five S_2/S_1, S_1/S_0 conical intersections (CI)[27,28] and eight T_2/S_1, T_1/S_0 intersystem crossings (ISC). All crossing points were optimized using the methods available in GAUSSIAN98. The optimization of both CIs and ISCs was found to be technically difficult due to the fact that the "sloped"[29] topography of these points[22,30] decreases the convergence efficiency. *For this reason, the reported structures represent a compromise between the quality of energy minimization on the upper state and the complete energy degeneracy between the two intersecting states*.

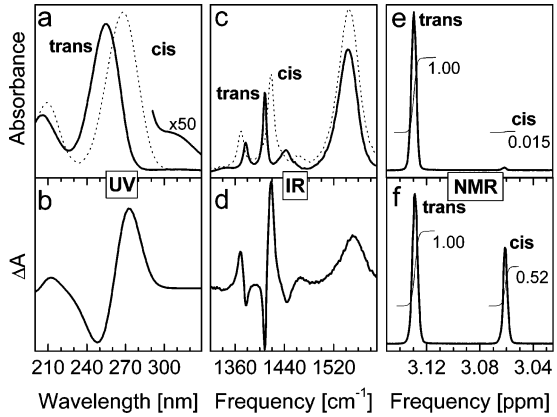

Figure 1. (a) Solid lines: UV-absorption spectrum of *trans*-NMTAA in deuterated water. (b) Difference absorption spectrum under UV-irradiation. (c) Solid line: FTIR absorption spectrum of *trans*-NMTAA before irradiation. (d) FTIR difference absorption spectrum under UV-irradiation. The dotted lines in (a) and (c) show the *cis*-NMTAA absorption spectra, which were constructed from the trans and the difference spectra. (e) NMR spectrum at room temperature before irradiation and (f) in photo equilibrium after 256 nm irradiation. The numbers indicate the normalized peak areas.

A S_2 MEP calculation was performed to connect the Franck−Condon point to the S_2 minimum and S_2/S_1 CI, using a two-root (S_1,S_2) state-average (0.5,0.5) CASSCF wave function. An S_1 MEP connecting the S_2/S_1 CI to one of the S_1 minimum has been computed using a two-root (S_0,S_1) state-average (0.5,0.5) wave function. Finally, for each S_1/S_0 CI and T_1/S_0 ISC a S_0 MEP connecting the chosen CI or ISC point to the S_0 reagent or product minimum was computed using a single-root wave function.

As stated before, energies of stationary points, CIs, ISCs, and selected points along the MEPs have been reevaluated using single-point calculations performed at the CASPT2 level of theory. For each geometry, a three-root (S_0,S_1,S_2) state-average (0.33,0.33,0.33) CASSCF wave function was used as reference function for evaluating the CASPT2 energies of the singlet states, while a two-root (T_1,T_2) state-average (0.5,0.5) wave function was used for the triplet states. Also, for each energy minimum on S_1 and T_1 a four-root (S_0,S_1,S_2,S_3 or T_1,T_2,T_3,T_4) state-average (0.25,0.25,0.25,0.25) CASSCF wave function was used as the reference function for evaluating the CASPT2 energies of third and fourth roots.

3. Experimental Results

3.1. Steady-State Absorption and Kinetic Studies. The solid lines in Figure 1a and c show the UV and infrared absorption spectra of *trans*-NMTAA in D_2O at room temperature. The S_2 state, which is due to a $\pi-\pi^*$ excitation (see below), gives rise to the main UV absorption band centered at 255 nm, while a much weaker shoulder at 305 nm is due to the S_1 state ($n-\pi^*$ transition). In the infrared spectrum, three prominent bands were of main interest in this study. They were assigned on the basis of a normal mode calculation on BLYP 6-31G(d) level (GAUSSIAN98), which was capable of reproducing approxi-

(20) Gonzalez-Luque, R.; Garavelli, M.; Bernardi, F.; Merchán, M.; Robb, M. A.; Olivucci, M. *Proc. Natl. Acad. Sci. U.S.A.* **2000**, *97*, 9379.
(21) De Vico, L.; Page, C. S.; Garavelli, M.; Bernardi, F.; Basosi, R.; Robb, M. A.; Olivucci, M. *J. Am. Chem. Soc.* **2002**, *124*, 4124.
(22) Bearpark, M. J.; Robb, M. A.; Schlegel, H. B. *Chem. Phys. Lett.* **1994**, *223*, 269.
(23) Celani, O.; Robb, M. A.; Garavelli, M.; Bernardi, F.; Olivucci, M. *Chem. Phys. Lett.* **1995**, *243*, 1.
(24) Andersson, K.; Malmqvist, P.-Å.; Roos, B. O. *J. Chem. Phys.* **1992**, *96*, 1218.
(25) Andersson, K.; Barysz, M.; Bernhardsson, A.; Blomberg, M. R. A.; Cooper, D. L.; Fülscher, M. P.; Graaf, C. D.; Hess, B. A.; Karlström, G.; Lindh, R.; Malmqvist, P.-Å.; Nakajima, T.; Neogrády, P.; Olsen, J.; Roos, B. O.; Schimmelpfennig, B.; Schütz, M.; Seijo, L.; Serrano-Andrés, L.; Siegbahn, P. E. M.; Stålring, J.; Thorsteinsson, T.; Veryazov, V.; Widmark, P.-O. *MOLCAS*, version 5.4, Lund University, Sweden, 2002.
(26) Frisch, M. J.; Trucks, G. W.; Schlegel, H. B.; Scuseria, G. E.; Robb, M. A.; Cheeseman, J. R.; Zakrzewski, V. G.; Montgomery, J. A., Jr.; Stratmann, R. E.; Burant, J. C.; Dapprich, S.; Millam, J. M.; Daniels, A. D.; Kudin, K. N.; Strain, M. C.; Farkas, O.; Tomasi, J.; Barone, V.; Cossi, M.; Cammi, R.; Mennucci, B.; Pomelli, C.; Adamo, C.; Clifford, S.; Ochterski, J.; Petersson, G. A.; Ayala, P. Y.; Cui, Q.; Morokuma, K.; Malick, D. K.; Rabuck, A. D.; Raghavachari, K.; Foresman, J. B.; Cioslowski, J.; Ortiz, J. V.; Baboul, A. G.; Stefanov, B. B.; Liu, G.; Liashenko, A.; Piskorz, P.; Komaromi, I.; Gomperts, R.; Martin, R. L.; Fox, D. J.; Keith, T.; Al-Laham, M. A.; Peng, C. Y.; Nanayakkara, A.; Gonzalez, C.; Challacombe, M.; Gill, P. M. W.; Johnson, B.; Chen, W.; Wong, M. W.; Andres, J. L.; Gonzalez, C.; Head-Gordon, M.; Replogle, E. S.; Pople, J. A. *Gaussian98*, revision A.7; Gaussian, Inc.: Pittsburgh, PA, 1998.
(27) Robb, M. A.; Garavelli, M.; Olivucci, M.; Bernardi, F.. In *Reviews in Computational Chemistry*; Lipkowitz, K. B., Boyd, D. B., Eds.; Wiley-VCH: John Wiley and Sons Inc.: New York, 2000; pp 87−146.
(28) Olivucci, M.; Robb, M. A.; Bernardi, F.. In *Conformational Analysis of Molecules in Excited States*; Waluk, J., Ed.; Wiley-VCH: John Wiley and Sons Inc.: New York, 2000; pp 297−366.
(29) Atchity, G. J.; Xantheas, S. S.; Ruedenberg, K. *J. Chem. Phys.* **1991**, *95*, 1862.
(30) Energies and energy gaps oscillate during the geometry optimization and never converge, or if energy gap tends to converge the energy increases endlessly. This behavior has been found to be associated with highly sloped conical intersections.

Table 1. Cis Concentrations c_{cis} in Photoequilibrium and Quantum Efficiencies of trans → cis Isomerization $\eta_{t\rightarrow c}$ for Different Irradiation Wavelengths Obtained from Kinetic and from Transient Absorption Measurements[a]

λ/nm	c_{cis}, %	$\eta_{c\rightarrow t}/\eta_{t\rightarrow c}$	$\eta_{t\rightarrow c}$ (kinetic), %	$\eta_{t\rightarrow c}$ (transient), %
256	34 (NMR)	2.3−3.1	40[b]	30−40
280	4.4 (NMR)	2.1−3.5	28	30−40
308	(14 ± 2)[c]	3−6	−	−

[a] The ratio $\eta_{c\rightarrow t}/\eta_{t\rightarrow c}$ was estimated form the concentrations in photoequilibrium and the absorption cross sections of *cis*- and *trans*-NMTAA. [b] The error due to the uncertainty in the photon flux is estimated to be 5 0%. [c] Determined by IR difference spectroscopy (calibrated by the NMR value at 256 nm).

mate frequencies, relative intensities, and energy shifts upon isomerization. The band at 1545 cm^{-1} is the amide II band, which is strongly blue-shifted with respect to matrix isolation spectra of NMTAA[31] and broadened due to strong interaction with the D_2O solvent. The band at 1409 cm^{-1} and the weaker band at 1372 cm^{-1} can best be characterized as "symmetric" and "antisymmetric" stretch motion of the C−C−N−C backbone. Both modes also involve an umbrella-like motion of the methyl groups (The extinction coefficients for *trans*-NMTAA are 12 400 L mol^{-1} cm^{-1} at 255 nm and 200 L mol^{-1} cm^{-1} at 1545 cm^{-1}). The changes in UV and infrared absorption due to UV irradiation are shown in Figure 1b,d. In the UV, a red-shift is observed for the $\pi-\pi^*$ absorption band, and this shift obscures any changes that may occur in the region of the $n-\pi^*$ band. In the IR vibrational spectrum, the trans band at 1409 cm^{-1} undergoes a blue-shift and gains in oscillator strength upon photoisomerization, while a red shift is observed for the 1372 cm^{-1} band. The amide II band of the cis species is stronger and peaks at slightly larger energies than the trans band. Kinetic measurements, based on both UV and FTIR absorption data, show an exponential decrease of the *trans*-NMTAA concentration and a simultaneous growth of the *cis*-NMTAA photoproduct. There are well-defined isosbestic points in the difference absorption spectra, which is an indication of simple two-state kinetics cis $\overset{h\nu}{\rightleftharpoons}$ trans. Indeed, due to the strongly overlapping UV-absorption bands of the two isomers, the photoreaction can take place in both directions, and a photoequilibrium between cis and trans species is eventually established. The *cis*-NMTAA concentration in the photostationary state under 256 nm irradiation is 34%, compared to only 1.5% in thermal equilibrium before irradiation (Figure 1e,f). Mainly due to the differences in the relative absorption cross sections of *cis*- and *trans*-NMTAA, their concentrations in photoequilibrium vary strongly as a function of irradiation wavelength, as shown in Table 1.[32] The table also shows the ratio of the quantum efficiencies for trans → cis and cis → trans isomerization, which can be determined directly from the concentrations in photoequilibrium and the absorption cross sections. Although associated with large error bars due to uncertainties in the photon flux, the estimates for the trans → cis isomerization quantum efficiency (20−40 for $\pi-\pi^*$ excitation) from the kinetic data is very similar to the more reliable value (30−40%) obtained from our transient measurements (see below).

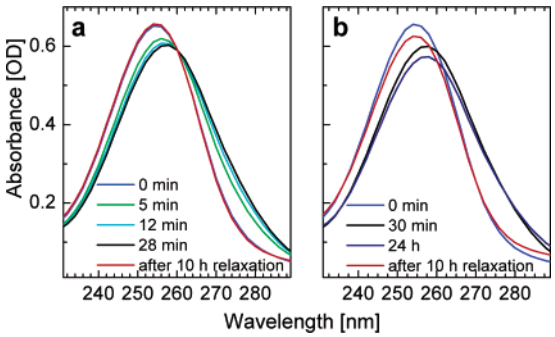

Figure 2. (a) UV-absorption spectra of NMTAA before irradiation (blue line, 98% trans) and after 5, 12, and 28 min of irradiation at 255 nm. After 10 h in the dark at room temperature the original absorption spectrum has completely recovered (red line). (b) Irradiation for much longer than 30 min leads to a very slow degradation of the sample without further isomerization and only partial recovery of the initial absorption spectrum after thermal relaxation.

In previous work sample degradation and trans → cis isomerization were found to occur with equal probability and their combined quantum efficiency was estimated to be 24%.[12] In contrast, we find very little to no degradation of our NMTAA samples during the time needed to reach photoequilibrium. When irradiation was stopped in photoequilibrium, the original trans absorption spectra completely recovered due to thermal relaxation back to trans (Figure 2a). Only after an irradiation dose that corresponds to approximately 50 photoexcitations per molecule did we observe an irreversible 5% loss and a small red shoulder in the UV absorption spectrum of NMTAA after thermal relaxation (Figure 2b). At the same time, however, no new vibrational bands could be detected in the FTIR spectrum.[33] Thus, we conclude that NMTAA in D_2O is photostable upon $\pi-\pi^*$ excitation with a quantum efficiency for decomposition below 0.1%. These findings are in agreement with recent measurements on small thio-substituted dipeptides.[5]

3.2. Time-Resolved Measurements. 3.2.1. UV−Vis Spectral Range. Transient absorption changes of an aqueous solution of *trans*-NMTAA were recorded over a wide spectral range and compared to the contribution of the pure solvent H_2O under identical conditions. Graphs a and b in Figure 3 show transients at two selected probe wavelengths (371 and 483 nm) after UV-excitation at 258 nm. The graphs are composed of two different data sets, one for delay times $\Delta t < 10$ ps (plotted on a linear scale) with a small temporal increment to facilitate detection of fast components and one for $\Delta t > 10$ ps (plotted on a logarithmic scale). At 371 nm an absorption increase is observed for the NMTAA solution (open circles) which rises within the time resolution of the setup and decays with a fast (1.1 ps) and a slow (260 ps) time constant. Both time constants can also be observed at a probing wavelength of 483 nm. However, the fast component has a smaller relative amplitude and now appears as a rise time. Pure H_2O also shows positive transient absorption at the two wavelengths (triangles), but these signals contain no comparable fast components. This rise in solvent absorption is attributed to the photoinduced formation of solvated electrons, with a lifetime on the order of microseconds in pure liquid

(31) Ataka, S.; Takeuchi, H.; Harada, I.; Tasumi, M. *J. Phys. Chem.* **1984**, *88*, 449.

(32) Since the irradiation wavelength can be changed without removing the sample from the FTIR spectrometer, the concentrations in photoequilibrium for different irradiation wavelengths can be determined with high accuracy (and independent of any spectrometer drifts) relative to the value at 255 nm by comparing the peak-to-peak differences in the FTIR-difference spectra shown in Figure 1d).

(33) Note, however, that the sample can be efficiently destroyed upon irradiation with an unfiltered low-pressure Hg lamp, which we attribute to excitation by light from the 193-nm line.

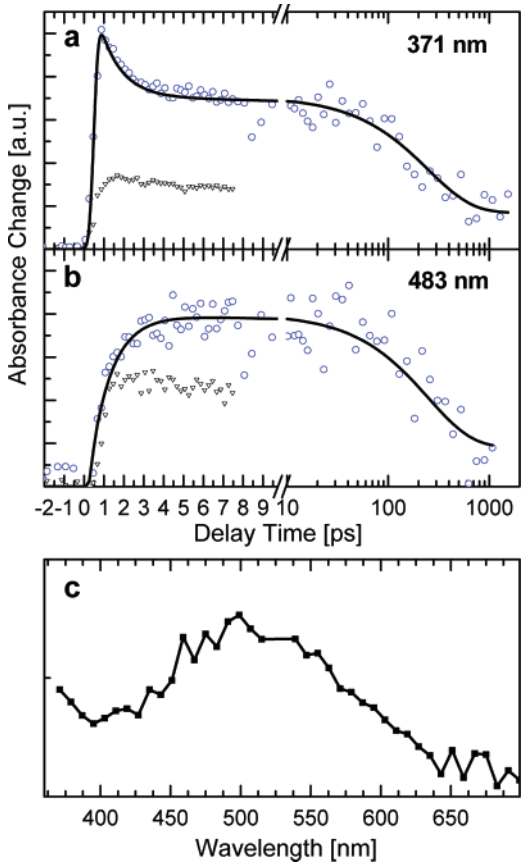

Figure 3. Transient absorption signals of NMTAA in H_2O (circles) and pure H_2O (triangles) at characteristic probe wavelengths of (a) 371 nm and (b) 483 nm, upon UV-excitation at 258 nm. The solid lines show double-exponential fits with timeconstants of 1.1 and 260 ps. (c) Spectrum associated with the 260-ps time constant in fits to a set of transients between 350 and 700 nm.

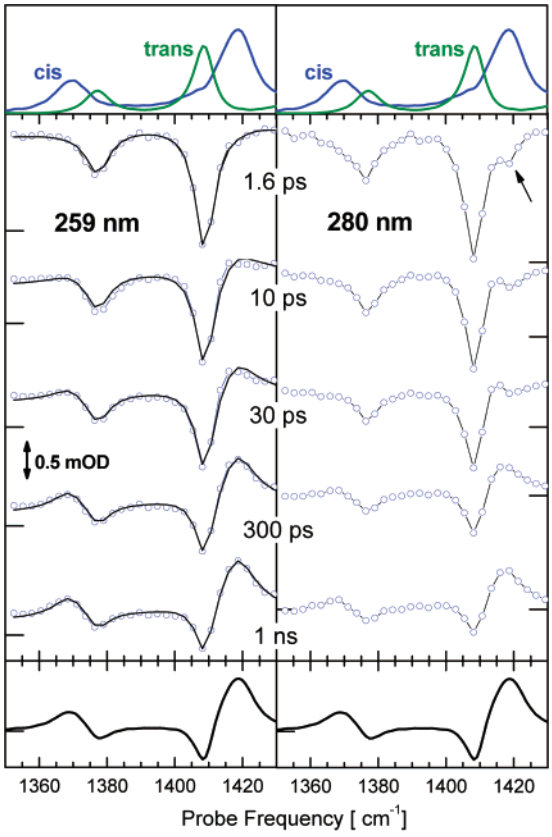

Figure 4. Magic angle transient infrared absorption spectra at different time delays after 259 nm (left) and 280 nm (right) excitation of NMTAA in D_2O. Thick black lines in the left column show least-squares fits using a linear combination of the cis and trans FTIR absorption spectra (shown on top). Horizontal ticks mark the zero lines. The FTIR difference absorption spectrum (bottom) is also shown for comparison.

water.[34,35] Their contribution to the signal of the concentrated NMTAA solution should be significantly smaller due to the high optical density and the resulting much shorter (<15 μm) effective sample thickness. The true size of the background signal can in fact be estimated from the long-delay offset in the NMTAA data, which is much smaller than for pure H_2O.

The transient measurements thus clearly identify absorption of an excited state of NMTAA with a lifetime of ~250 ps. A pronounced maximum around 500 nm is found in the decay-associated spectrum related to this slow time constant (Figure 3c), which may be interpreted as the spectral characteristics of this long-lived excited-state band. Unfortunately, fast-varying solvent contributions to the signal do not allow an unambiguous identification of the spectrum associated with the 1.1 ps time constant. Overcompensatory effects by strong positive contributions from the solvated electron and the excited-state absorption of NMTAA may also obscure stimulated emission signals, which could not be identified in the accessible spectral range between 300 and 1000 nm.

3.3.2. Mid-infrared Spectral Range. Changes in the mid-infrared absorption at different time delays after 259 nm excitation of *trans*-NMTAA are shown in the left column of Figure 4.

Apart from a positive offset, the transient spectra at very early times after photoexcitation have the same shape as that of the FTIR absorption spectrum of *trans*-NMTAA. Within the first 30 ps the initial bleaching signal is reduced to little more than half of its original size, and positive absorption bands grow in at the spectral positions of the *cis*-NMTAA vibrations. This dynamics subsequently continues on a much slower time scale. After 1 ns, the difference spectra fully reproduce the FTIR difference spectrum, and no further changes are observed for longer time delays.[39] These results were found to be independent of concentration in the range of 50−250 mM.

The right column of Figure 4 shows transient spectra recorded for 280 nm excitation, where the *cis*-NMTAA absorption is approximately 5−10 times stronger than that of *trans*-NMTAA (see Figure 1). Thus, although only a small fraction of the molecules are initially in the cis-conformation (≤2% cis at room temperature), these do contribute to the transient signal, when

(34) Hart, E. J.; Boag, J. W. *J. Am. Chem. Soc.* **1962**, *84*, 4090.
(35) Alfano, J. C.; Walhout, P. K.; Kimura, Y.; Barbara, P. F. *J. Chem. Phys.* **1993**, *98*, 5996.
(36) The isomerization quantum yields were determined in the following way: The FTIR trans-absorption spectrum was fit to the magic angle transient signal at 1-ps delay (maximum bleach) by simple rescaling. This determines the amount of initially excited trans species. Next, a FTIR trans−cis difference spectrum was rescaled to fit to the 1-ns transient spectrum. The rescaled absorption spectrum A, multiplied by a variable factor $\eta_{t\rightarrow c} \leq 1$ can now be added to the rescaled difference spectrum D, until a smooth product-spectrum P with symmetric line shapes is obtained; $\eta_{t\rightarrow c}$ is the quantum efficiency of isomerization. This method yields $\eta_{t\rightarrow c} = 0.35 \pm 0.05$. At 280 nm, where *cis*-NMTAA is also excited, the product spectrum is proportional to $D + (\eta_{t\rightarrow c} - \eta_{t\rightarrow c}n_C/n_T)A$, were n_C/n_T is the ratio of initially excited cis and trans molecules.
(37) Hamm, P.; Ohline, S. M.; Zinth, W. *J. Chem. Phys.* **1997**, *106*, 519.
(38) Sieler, G.; Schweitzer-Stenner, R. *J. Am. Chem. Soc.* **1997**, *119*, 1720.

exciting at this wavelength. Indeed, immediately following excitation, a bleaching signal is now also observed at the cis transition energies (see array, right column in Figure 4). This signal increased during long series of measurement as a result of cis accumulation but never exceeded 10−20% of the trans bleaching signal. Apart from the additional contribution due the excitation of *cis*-NMTAA no significant differences in the dynamics after excitation at the two wavelengths were observed. The larger change in amplitude of the signal for 280 nm excitation is due to the fact that cis → trans isomerization diminishes the trans → cis difference spectrum at long time delays. Taking this into account, we find that the trans → cis isomerization quantum yields for 280 and 259 nm excitation are equal within experimental error and lie in the range of 30−40%.[36]

To extract the relevant time scales involved in the dynamics, the magic angle signals for 259-nm excitation were analyzed using singular value decomposition (SVD). The resulting basis spectra contain no features that do not already appear in the steady-state absorption spectra of *cis*- and *trans*-NMTAA. The corresponding time traces can be fit simultaneously to a biexponential function, yielding global time constants of 8.5 ± 0.5 and 250 ± 20 ps.

We could not identify any vibrational bands that may be assigned to NMTAA in an electronically excited state. The IR absorption bands of these species may either have shifted out of the spectral window used for detection, or their distribution may be so broad that their absorption remains hidden in the unstructured background signal. A strong spectral shift could be caused by the fact that all the normal modes in the investigated spectral region include stretch motion of the central C−N bond, which have a significantly reduced bond order in the electronically excited states in which the molecule can isomerize (see below). Indeed we found that the transient spectra can be well reproduced by simply fitting the dataset with linear combinations of the cis and trans FTIR spectra (solid black lines in Figure 4). The quality of the fits is very good with only small deviations at intermediate delays, where there is a small red shift of the product absorption band near 1420 cm^{-1} with respect to the FTIR spectrum of *cis*-NMTAA. This red-shift is maybe better seen with respect to the bleaching signal of *cis*-NMTAA in the spectra recorded upon 280 nm excitation (right column in Figure 4) and is a typical signature of a (cis) molecule at a more elevated temperature. It arises from anharmonic coupling of the high energy mode to low-frequency vibrations that have become excited thermally (or nonthermally) as a result of photoexcitation and energy dissipation.[37] Given the large amount of energy per normal mode that is delivered to the molecule by a 259-nm photon, the observed shifts are, however, surprisingly small. Our transient infrared measurements thus appear to be sensitive only to ground-state molecules that have dissipated most of the excitation energy. They monitor the arrival of

(39) The background underlying the NMTAA signal has two origins: A broad, unstructured positive signal, which decays to a small, constant value within approximately 10 ps is also observed for pure D_2O. The intensity of this background signal changes when the sample cell is moved, suggesting contributions from the cell windows. The main cause for the long-time background signal is, however, the temperature rise in D_2O as the excess photon energy is dissipated to the solvent. FTIR measurements show that a small increase in temperature (1 K) leads to a positive, nearly flat difference signal in the 1300−1450 cm^{-1} region, which can be easily subtracted as a linear background from the transient data. It stays constant at delay times longer than 100 ps, indicating the end of the main energy dissipation.

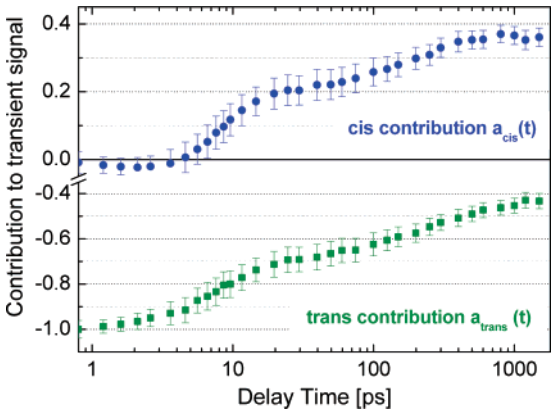

Figure 5. Time-dependent contributions of cis and trans absorption spectra in a least-squares fit $a_{cis}A_{cis}(\nu) + a_{trans}A_{trans}(\nu)$ + linear background to the magic angle transient spectra between 1350 and 1450 cm^{-1}. $A_{cis}(\nu)$ and $A_{trans}(\nu)$ denote the FTIR absorption spectra, which were scaled to yield $a_{trans} = -1$ at the earliest pump probe delay. The linear term $c(t)\nu + d(t)$ was added in the fit to account for the time-dependent background signal, caused mainly by the temperature rise in the D_2O solvent. Error bars represent confidence intervals.

population in either the relaxed cis or trans conformation of NMTAA, and the observed dynamics is therefore due to the joint processes of electronic relaxation and vibrational cooling.

Figure 5 shows the contributions of cis and trans species to the transient spectra at different time delays, extracted from the fits using their ground-state absorption spectra. It can be seen that both the recovery of the initial trans ground state and the formation of *cis*-NMTAA occur on two distinct time scales, with time constants compatible with those obtained from the SVD analysis (8.5 and 250 ps). About 30% of the initially excited trans population returns to the (cold) trans ground state within the first 20−30 ps following the 259-nm pump pulse. At the same time, another 15−20% is converted into ground-state *cis*-NMTAA. This early recovery of the IR absorption bands of cold ground-state species indicates fast electronic decay and very efficient excess energy dissipation from the thioamide to the solvent. A strong interaction of NMTAA with D_2O is already apparent from the broad amide II absorption band that is strongly blue-shifted compared to the matrix-isolated molecule,[31] and efficient energy dissipation could take place, for example, via dipolar coupling to the D_2O molecules of the first hydration shell, as is the case of NMA in water,[38] and more directly through intermolecular hydrogen bonds. As a result, the 8−9 ps time constant very probably reflects the cooling of photoexcited NMTAA in deuterated water.

Further reduction of the initial *trans*-NMTAA bleach and the growth of the *cis*-NMTAA absorption bands take place on a much slower time scale which is comparable to the time of excited-state decay in the visible measurements. Just as on the fast time scale, roughly 2 times more trans species than cis species are formed in the slow process. Overall, 35−40% of the excited NMTAA molecules are converted into cis, and the remaining molecules return to the ground state in the trans conformation.

4. Photochemical Reaction Path Computations

The only energy minima located on the S_0 potential energy surface correspond to *trans*-NMTAA and *cis*-NMTAA. These are planar structures featuring C_s symmetry with the cis stereoisomer located 1.9 kcal mol^{-1} above the trans stereoiso-

Table 2. Molecular Orbital Occupation of *trans*-NMTAA in the S_0, S_1, and S_2 States: Only the p-Type Sulfur Lone Pair and the π/π^* Orbitals Are Depicted[a]

	sulfur lone pair	π	π	π^*
S_0	1.998	1.981	1.955	0.064
S_1	1.000	1.993	1.998	1.008
S_2	1.995	1.972	1.413	0.616

[a] Occupations were calculated using a three roots (S_0, S_1, S_2) state average (0.33, 0.33, 0.33) CASSCF wave function.

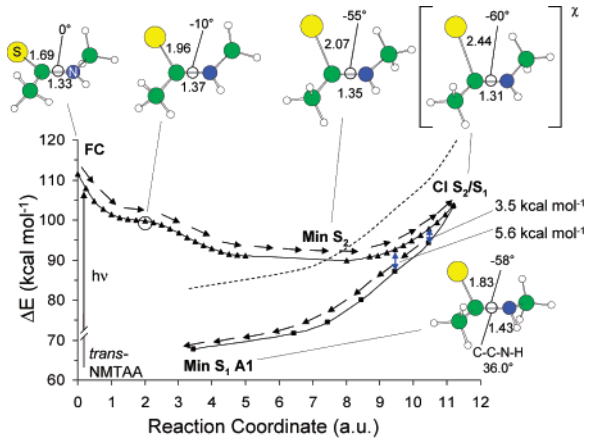

Figure 6. **FC → Min S_2 → CI S_2/S_1** and **CI S_2/S_1 → Min S_1 A1** paths computed at the CASPT2//CASSCF level of theory. The reaction coordinate is in mass-weighted Cartesians (a.u. = amu$^{1/2}a_0$). Full triangles and full squares represent S_2 and S_1 energies, respectively. C−S and C−N bond distances are given in Å; the S−C−N−C dihedral angle is given in degrees. For **Min S_1 A1** the C−C−N−H angle is also reported. The χ symbol indicates the CI. The dashed line represents the estimated shift in the position of the n−π^* state due to solvent effects (see section 5.1).

mer. Two fully asymmetric S_0 transition states (**TS S_0 A1** and **TS S_0 B1**) describe the trans → cis *thermal* isomerization reaction. They are located 24.9 and 20.7 kcal mol^{-1} above *trans*-NMTAA, respectively. These values compare very well with *cis*-NMTAA concentrations of 4% at room temperature and a free activation enthalpy of 22 kcal mol^{-1} in dilute CCl_4 solution.[40] Notice that the presence of the pyramidalized nitrogen center allows for the existence of one enantiomeric form (**TS S_0 B2** and **TS S_0 A2**) for each transition state.

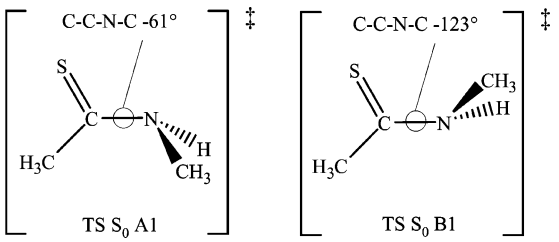

Wave function analysis at *trans*-NMTAA establishes that the S_2 state corresponds to a $\pi-\pi^*$ excitation, while the S_1 corresponds to a n−π^* excitation (see Table 2).

4.1. Excited-State Relaxation. As shown in Figure 6, relaxation from the Franck−Condon point (**FC**) of *trans*-NMTAA is dominated by C−S bond expansion: the C−S bond passes from 1.69 to around 1.96 Å, while the C−N bond stretches from 1.33 to 1.37 Å. Later along the same relaxation path, the sulfur atom is lifted out of plane as the thiocarbonyl carbon starts to pyramidalize. At **Min S_2** the C−S bond distance is 2.07 Å, while the C−N bond distance goes back to 1.35 Å; the S atom makes a −55° dihedral angle with the carbon−nitrogen frame which, in turn, remains nearly planar. A further expansion of the C−S bond of **Min S_2** leads to a S_2/S_1 conical intersection (**CI S_2/S_1**) located ca. 14 kcal mol^{-1} higher than the minimum.

Relaxation from **CI S_2/S_1** to the S_1 potential energy surface is achieved via a path dominated by back-contraction of the C−S bond length to 1.83 Å and expansion of the C−N bond distance to 1.43 Å. During the relaxation the thiocarbonyl carbon center remains pyramidalized while the originally planar nitrogen center pyramidalizes. The existence of two pyramidalized centers implies the existence of two diastereoisomers for the S_1 minimum. These have indeed been located and are referred to as **Min S_1 A1** (A stands for S,R) and **Min S_1 B1** (B stands for S,S). As a consequence, the low-lying region of the S_1 potential energy surface is spanned by two flat "valleys" (Paths A and B) that originate from the diastereoisomers **Min S_1 A1** and **Min S_1 B1**, respectively. Starting from **Min S_1 A1** on Path A we were able to map the entire conformational space corresponding to the torsional deformation about the central C−N bond. As shown in Figure 7, this path intercepts three conformational minima and three conformational transition states, in the order **Min S_1 A1 → TS S_1 A1 → Min S_1 A2 → TS S_1 A2 → Min S_1 A3 → TS S_1 A3**. From **TS S_1 A3** the molecule goes back to **Min S_1 A1**.

Transition between Path A and Path B is possible through inversion transition states. For instance, the passage between **Min S_1 A1** and **Min S_1 B1** is driven by a transition state (**TS S_1 Pyr1** in the Supporting Information) located 2.6 kcal mol^{-1} higher than **Min S_1 A1**. As reported in Figure 7 and similar to Path A, Path B comprises three conformational minima and three conformational transition states (in the order **Min S_1 B1 → TS S_1 B1 → Min S_1 B2 → TS S_1 B2 → Min S_1 B3 → TS S_1 B3**. From **TS S_1 B3** the molecule goes back to **Min S_1 B1**). The maximum energy difference between the entire set of minima and transition states is ca. 3.5 kcal mol^{-1}; thus, at room temperature, the molecule can explore the entire conformational space of both Paths A and B.

4.2. Relaxation to the Ground State. Decay to S_0 occurs via four different CIs. Two CIs are located along Path A (**CI S_1/S_0 A1** and **CI S_1/S_0 A2**) and two along Path B (**CI S_1/S_0 B1** and **CI S_1/S_0 B2**). All CIs are characterized by a S−C−N angle of ca. 90°. As mentioned in section 2.2, these energy surface crossings are difficult to locate, and therefore, the structures reported are the best compromise between the requirement of stability and degeneracy. All decay channels are located in the range of 9.7−16.3 kcal mol^{-1} above **Min S_1 A1**.[41] As reported in Figure 7, relaxation path computations indicate that the photochemical outcome of an S_0 relaxation process depends on the specific decay channel (i.e., the specific surface crossing) prompting the relaxation. Remarkably, we found that only **CI**

(40) Walter, W.; Schaumann, E. *Chem. Ber.* **1971**, *104*, 3361.

(41) Reported energies for CIs represent the mean between the S_1 and S_0 CASPT2 energy values reported in Table 5S in Supporting Information. Energy degeneracy was achieved at the CASSCF level of theory, but the CASPT2 treatment split the two energies. The mean values represent a good approximation of the energy of the CI.

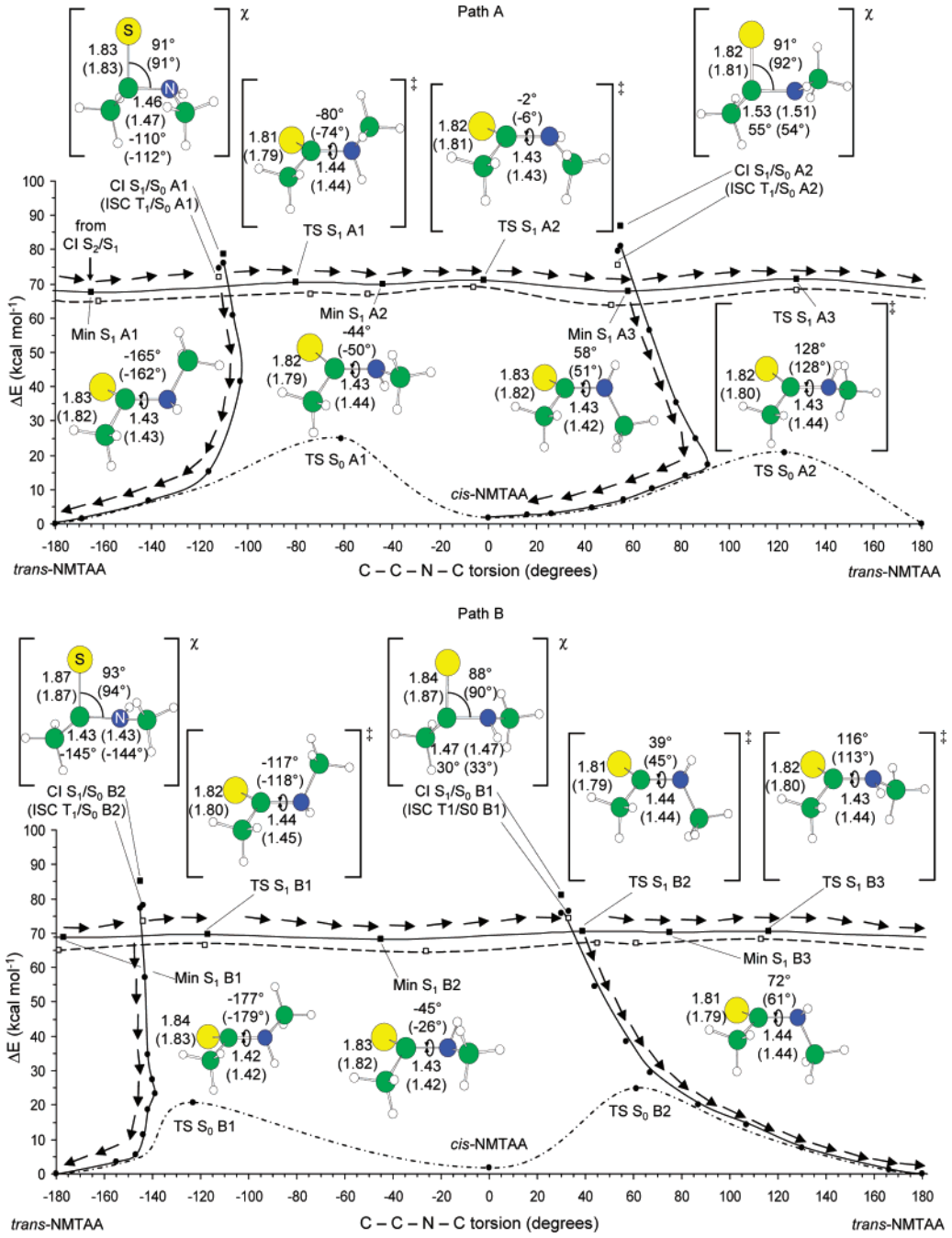

Figure 7. S_1 (full line), T_1 (dashed line), and S_0 (dot−dashed line) isomerization paths and $S_1(T_1) \rightarrow S_0$ relaxation paths (full line) computed at the CASPT2//CASSCF level of theory. Full circles, full squares, and open squares represent S_0, S_1, and T_1 energies, respectively. C−S and C−N bond distances are in Å and C−C−N−C dihedral angles, in degrees. For the CIs and the ISCs the S−C−N angle is also given. Values in parentheses refer to T_1. While the C−C−N−C dihedral angle has been chosen as the internal coordinate that represents the trans−cis isomerization path, relaxation on S_0 is also characterized by planarization at the carbon and nitrogen centers. The nitrogen atoms of all structures along Path A are in the R conformation, while on Path B the nitrogens have an S conformation. The χ symbol indicates the CIs and the ISCs, the ‡ indicates the transition states.

S_1/S_0 A2 gives access to the cis product (*cis*-NMTAA), while decay at the other three CIs results in production of the initial trans molecule. One may explain this result by comparing the value of the C−C−N−C dihedral angle along a specific relaxation path to the value of the same dihedral angle for the ground-state transition structures. In fact, these define the ridge between the cis and trans valleys on the S_0 potential energy surface (see Figure 7).

The analysis of the relaxation coordinates starting at **CI S_1/S_0 A1** and **CI S_1/S_0 B2** (C−C−N−C dihedral angles of −110° and −145° respectively) shows that the initial relaxation is dominated by replanarization of the thiocarbonyl carbon center. As shown in Figure 7, after replanarization the molecule finds itself in the trans valley and goes back to the trans form. In contrast, the analysis of the relaxation coordinates starting at **CI S_1/S_0 A2** and **CI S_1/S_0 B1** (C−C−N−C dihedral angle of 55° and 30° respectively) shows that, due to the steric repulsion between the two fairly eclipsed methyl groups, thiocarbonyl carbon replanarization occurs simultaneously to a C−C−N−C dihedral angle increase of ca. 35°. For this reason, when the relaxation starts at **CI S_1/S_0 A2**, the molecule achieves a dihedral angle of ca. 90° that is lower than the 123° angle of **TS S_0 A2**

Table 3. Comparison of Experimental and CASPT2//CASSCF Calculated Absorption Wavelengths and CASSCF Oscillator Strengths[a]

	experimental			calculated			
	n–π^*	π–π^*	*f*	n–π^*	*f*	π–π^*	*f*
absorption trans	305 (94)	255 (112)	2.5×10^{-1}	366 (78)	1.43×10^{-2}	257 (111)	3.06×10^{-1}
absorption cis		268 (107)		374 (76)	0.92×10^{-2}	267 (107)	3.26×10^{-1}
fluorescence[b]						796 (36)	

[a] The calculated $S_2 \rightarrow S_0$ fluorescence maximum is also reported. Data are in nm, while kcal mol^{-1} values are given in brackets. [b] Vertical energy difference between S_2 and S_0 energy values of **Min S_2**.

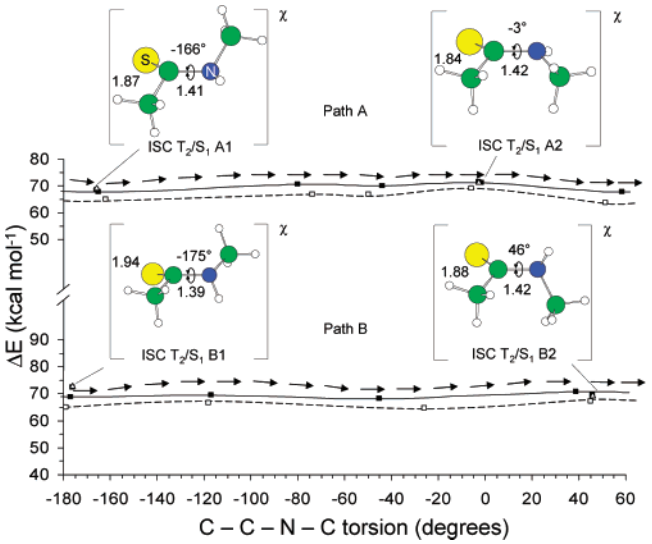

Figure 8. T_2/S_1 intersystem crossings computed at the CASPT2//CASSCF level of theory. Full squares, open squares, and open triangles represent S_1, T_1, and T_2 energies. Geometrical parameters, symbols, and lines are as in Figure 7.

and right on top of the cis valley. Thus, the cis form is generated. In contrast, when relaxation starts at **CI S_1/S_0 B1**, after thiocarbonyl carbon replanarization the structure displays a dihedral angle of ca. 65° which is larger than the dihedral angle of **TS S_0 B2** and right on top of the trans valley. *In conclusion our relaxation path analysis shows that relaxation from three out of four decay channels leads to the trans form.*

4.3. Population and Decay of the Triplet States. Our computations establish the existence of triplet trans−cis isomerization pathways that, ultimately, lead to the same photoproduct distribution. In fact, as shown in Figure 7, the structure of the T_1 energy surface is analogous to the one seen for S_1. Indeed, we have been able to locate six different T_1 conformers (three along Path A and three along Path B). These conformers may decay to S_0 via four different T_1/S_0 ISCs (two for Path A and two for Path B) featuring a geometrical structure very close to the corresponding S_1/S_0 CIs described above. Thus, ground-state relaxation from T_1 may substantially occur along the same paths already described for the S_1 relaxation. However, notice that the energy difference between the T_1 minima and the ISCs is considerably smaller than the energy difference between the S_1 minima and the S_1/S_0 CIs.

In principle efficient population of the T_1 energy surface may occur via intersystem crossing from S_1 to T_2 followed by internal conversion from T_2 to T_1. Indeed, as shown in Figure 8 the S_1 conformers can access the T_2 state via four different T_2/S_1 ISC channels located near the region of **Min S_1 A1**, **TS S_1 A2**, **Min S_1 B1**, and **TS S_1 B2**. Following the El-Sayed rules for intersystem crossings,[42,43] the T_2 state (corresponding to a triplet π−π^* excitation) can be accessed quite efficiently from a degenerate singlet n−π^* state. Since, in the same region, the T_2 and T_1 potential energy surfaces are substantially degenerate,[44] we assume that the T_1 state is readily accessed, allowing for the efficient population of the six different T_1 conformers of Figure 7.

4.4. Comparison with Spectroscopic Data. To validate our computational strategy (see section 2.2), we compare the experimental absorption and phosphorescence energies with the corresponding calculated data. Absorption maxima were calculated as the difference between the S_1 (for the $S_0 \rightarrow S_1$ transition) or S_2 (for the $S_0 \rightarrow S_2$ transition) energy and the S_0 energy at *trans*-NMTAA and *cis*-NMTAA. The resulting values are summarized in Table 3.

It can be seen that the π−π^* absorption and the absorption red-shifts observed when passing from the trans to the cis form are well reproduced. On the other hand, there is a large discrepancy between the calculated and the observed n−π^* absorption maximum, possibly because we did not consider solvent effects in our computation. Indeed, S_0, S_1, and S_2 have calculated dipole moments of 4.9, 2.7, and 5.3 D, respectively. Thus a polar solvent is expected to induce a similar stabilization in S_0 and S_2 (since these states have roughly the same dipole moment). On the other hand, the stabilization effect on S_1 is expected to be smaller, due to the lower dipole moment of this state. Previous works[45] showed that a quite sophisticated treatment of the solvent bulk is needed to predict n−π^* excitation energies in good agreement with the experimental data.

We also tried to reproduce the phosphorescence maximum recorded in a methanol:ethanol low-temperature glass.[11] For this purpose, the phosphorescence maximum was calculated as the energy difference between T_1 (for the $T_1 \rightarrow S_0$ transition) or T_2 (for the $T_2 \rightarrow S_0$ transition) and S_0 at different structures as reported in Table 4. The calculated energy differences between T_1 and S_0 at the optimized geometry of the various energy minima on T_1 are not consistent with the experimental value. However, since the experiment was carried out in the constrained environment of a cold glass, one can assume that the molecule had sufficient space only to relax along the stretching coordinates (e.g. it could not relax along pyramidalization coordinates) and that radiative decay was the only way for the molecule to go back to S_0. This view is supported by the fact that the calculated $T_1 - S_0$ energy difference at the **Min T_1 Planar**

(42) El-Sayed, M. A. *J. Chem. Phys.* **1964**, *41*, 2462.
(43) Gilbert, A.; Baggot, J. *Essentials of Molecular Photochemistry*; Blackwell Scientific Publications: Oxford, 1991.
(44) For example, the energy difference between the T_2 and T_1 states at the T_2/T_1 ISCs is in the range 1.7−4.8 kcal mol^{-1}. See Table 5S in Supporting Information.
(45) Adamo, C.; Barone, V. *Chem. Phys. Lett.* **2000**, *330*, 152.

Table 4. CASPT2//CASSCF Calculated Maxima of Phosphorescence for Different Molecular Geometries and Experimental Values Observed in a Methanol:Ethanol Low-Temperature Glass[a]

experimental value[11]	calculated	structure	transition
485 (59)	757−945 (38−30)[b]	**Min T_1 A1 − B3**	$T_1 \rightarrow S_0$
	605−727 (47−39)[b]	**Min T_1 A1 − B3**	$T_2 \rightarrow S_0$
	426−448 (67−64)[b]	**Min T_1 A1 − B3**	$T_1 \rightarrow S_0$ nonvertical[c]
	470 (61)	**Min T_1 Planar Trans**	$T_1 \rightarrow S_0$
	462 (62)	**Min T_1 Planar Cis**	$T_1 \rightarrow S_0$

[a] Data are in nm, while kcal mol^{-1} values are given in brackets. [b] Data represent the range of the phosphorescence maximum calculated for the various minima on T_1 energy surface. [c] These values were calculated comparing T_1 energies of the **Min T_1 A1 − B3** minima with the S_0 energy of *trans*-NMTAA.

Trans and **Min T_1 Planar Cis** are in good agreement with the value of λ_{max} for the observed phosphorescence.

We also investigated the possible origins of the visible transient absorption signals (Figure 3c). The S_1/S_2 transition being energetically out of the recorded range, we calculated the singlet fourth root of each S_1 minimum and the triplet third and fourth roots of each T_1 minimum. (Results are reported in Table 7S in the Supporting Information.) As for the n−π^* excitations the computed $S_1 \rightarrow S_3$ or $T_1 \rightarrow T_3$ absorption will be shifted by a polar solvent due to the higher dipole moment of S_3 and T_3 (both $\pi-\pi^*$ states) with respect to S_1 and T_1. With the rough assumption that the energy shift would be similar to the one reported for n−π^* excitations, one can estimate the absorption wavelengths of the S_1 and T_1 minima (see Table 7S in the Supporting Information). Remarkably these values are in the range of those reported in Figure 3c; in particular, at least one minimum per Path (**Min S_1 A3**, **Min S_1 B1**, **Min T_1 A1**, **Min T_1 B2**) shows an absorption wavelength in the 500-nm region, along with a not-negligible calculated oscillator strength. Unfortunately this analysis cannot distinguish between S_1 or T_1 absorptions.

5. Discussion

Excited-state vibrational bands do not appear in our transient infrared spectra of photoexcited NMTAA, and well-defined bands are only observed at, or very near, the spectral positions of the room-temperature absorption bands of *cis*- and *trans*-NMTAA. Thus, the IR experiment provides information about the return of the photoexcited population to the two isomeric ground-state minima. Two distinct time scales of approximately 8 and 250 ps are observed for both the formation of *cis*-NMTAA and the recovery of *trans*-NMTAA. On both time scales, the same branching ratio between the two isomers is found, with a cis yield of approximately 30−40%. The UV−visible measurements yield complementary information on the dynamics in the electronically excited states, revealing that the 250-ps time constant represents the lifetime of an electronically excited state with an absorption band near 500 nm. These findings in combination with the computational results of section 4 provide a detailed picture of the mechanism underlying the photoisomerization of *trans*-NMTAA.

5.1. Fast Relaxation Dynamics. The IR experiment shows that 50% of the exited molecules relax to the ground state of either *cis*- or *trans*-NMTAA within a few picoseconds after excitation. This implies that isomerization and electronic relaxation from the initially excited $\pi-\pi^*$ state must take place on a faster time scale. Although our computations reveal that a S_2/S_1 conical intersection is located relatively high in energy with respect to **Min S_2**, suggesting a too-long S_2 lifetime, the analysis of the S_2 relaxation path indicates that fast radiationless decay may still occur since:

(i) The S_2 and S_1 surfaces become nearly degenerate well before the conical intersection. In fact, already at a point located only 2.8 kcal mol^{-1} above **Min S_2** there is an energy gap of only 5.6 kcal mol^{-1} (see Figure 6). Thus, one may assume that the nonadiabatic transition from one surface to the other starts to occur before the intersection.

(ii) Both position and relative energy of **CI S_2/S_1** are expected to be sensitive to the solvent environment, which can affect (e.g., lower or remove) the energy barrier controlling the decay. This effect is consistent with the solvent dependence of the S_1 absorption maximum discussed above and can roughly be estimated in terms of the difference between the experimental (in solution) and the calculated (in vacuo) n−π^* excitation energies (see Table 3). As shown in Figure 6, the crossing point moves close to the S_2 minimum when the resulting energy of ∼15 kcal mol^{-1} is added to the S_1 curve (dashed line). Another considerable solvent effect has been documented in NMA, the carbonyl analogue on NMTAA,[46] where the calculated C−O and C−N bond distances for $\pi-\pi^*$ differ significantly between vacuum and solution; indeed, in vacuo the C−O bond of NMA lengthens more than the C−N one, consistent with what we found for C−S versus C−N in NMTAA (see above). On the other hand, in solution the C−N bond expansion is greater than that of the C−O bond, as also indicated by resonance Raman data.[47] This has been attributed mainly to a more elongated C−O bond in the electronic ground state due to hydrogen bonding. While the relative C−N and C−S contributions to the initial relaxation path appear to change from the gas phase to solution and may be different in amides and thioamides, such effects clearly deserve further research efforts to be fully understood.

Notice that the prediction that initial relaxation on S_2 is dominated by C−N and C−S bond expansion (and not by torsional deformations) is consistent with the resonance Raman spectra recorded on NMA, where torsional modes are not enhanced.[15] It is also consistent with our observation that the quantum efficiency of isomerization does not depend on the irradiation wavelength (259 or 280 nm), which indicates that the initial excess energy plays no role in the trans−cis photoisomerization.

According to the above discussion the photoreaction must be determined by events occurring at lower energy. In fact, trans → cis isomerization motion is predicted to occur predominantly on the S_1 (and/or T_1) potential energy surface, where the molecule can sample all torsional angles without having to overcome significant energy barriers (see Figure 7). This can also explain the observation of trans−cis isomerization upon direct excitation of the S_1 state at 308 nm (n−π^* transition). From S_1 (or T_1) fast relaxation to the ground state is possible via four CIs (ISCs) that predetermine the final conformation adopted by the molecule. Indeed, if we make the rough assumption that the four different S_1/S_0 CIs have the same probability of being accessed, we can estimate a quantum yield for the trans → cis process close to 25%. This is remarkably

(46) Markham, L. M.; Hudson, B. S. *J. Phys. Chem.* **1996**, *100*, 2731.
(47) Asher, S. A.; Chi, Z.; Li P. *J. Raman Spectrosc.* **1998**, *29*, 927.

close to the measured quantum efficiency of 30−40%. We stress that the same conclusions are drawn if one considers decay from T_1 via the four T_1/S_0 intersystem crossing points documented above. Thus, the involvement of a "triplet" pathway cannot be excluded (see below).

The solvent is expected to have a similar effect on all four S_1/S_0 CIs (and the four T_1/S_0 ISCs), since the calculated dipole moments remain more or less at the value of *trans*-NMTAA along the isomerization path. This implies that the energy barrier between minima and intersection points should be higher in water than calculated in vacuo, while there is no evidence that one decay route may become preferred.

5.2. Slow Relaxation Dynamics. Half of the photoexcited molecules follow an ultrafast relaxation pathway back to the ground state. An approximately equal fraction of NMTAA relaxes much more slowly with a time constant of 250 ps. The observation of excited-state absorption with the same lifetime clearly shows that this slow dynamics is due to population trapping in an electronically excited state, which subsequently relaxes nonradiatively. However, just as in the fast process, the ratio of cis and trans yield is approximately 1:2, which indicates a similar relaxation pathway on both time scales. Our computational results offer two different explanations:

(i) Branching and population trapping occur on the S_2 surface, in which case the 250-ps time constant may be proportional to the time required to surmount the barrier between **Min S_2** and **CI S_2/S_1** (or a decay region close to it). Subsequent relaxation and isomerization would then be identical for temporarily trapped molecules and for the molecules that reach the $S_2 \rightarrow S_1$ decay point directly (e.g., impulsively).

In this case, however, fluorescence (predicted at a wavelength of 800 nm, see Table 3) should be observable from S_2, even in the presence of nonradiative relaxation with a rate of 250 ps^{-1}. In agreement with earlier work,[48,12] we were not able to detect any fluorescence from NMTAA in the 300−850-nm region, which, given the sensitivity of our setup, excludes trapping in a state with an oscillator strength $\geq 5 \times 10^{-2}$ for the transition to S_0 or implies a much smaller energy difference (i.e. emission at $\lambda \geq 850$ nm) between the excited-state minimum and the ground state. Note, however, that no stimulated emission could be detected in a spectral window up to 1000 nm. Furthermore, the 1-ps rise time in the transient signal at 483 nm and the corresponding fast decay at higher energies are rather untypical for spectral dynamics due to vibrational cooling (in the S_2 state), for which one would expect a blue-shift of the excited-state absorption. The 1-ps dynamics is therefore more likely due to electronic relaxation, suggesting that population trapping occurs after relaxation from S_2 to S_1.

(ii) Population trapping occurs on S_1 or T_1. This implies that an initial vibrationally hot S_1 population, produced by $S_2 \rightarrow S_1$ decay, either immediately decays to S_0 (giving rise to the fast time constant) or undergoes internal vibrational energy redistribution and gets temporarily trapped in the S_1 or T_1 excited state.

According to this scenario, competition between immediate electronic relaxation and cooling in the excited state would be at the origin of the two reaction regimes. An alternative scenario involves branching of the S_1 population that decays directly either to S_0 via the S_1/S_0 intersections or to T_2 via the T_2/S_1 crossings. The T_2 population would then decay to S_0 via the T_2/T_1 and T_1/S_0 crossings in a somehow slower process. Indeed, the observation of blue-green phosphorescence from NMTAA in a low-temperature glass by Tasumi et al.[11] could be an indication for the involvement of a triplet pathway. Notice that, as respectively documented in Figures 7 and 8, there are the same numbers of $S_1 \rightarrow T_2$ and $S_1 \rightarrow S_0$ decay channels and that they have similar energies. It is therefore not unlikely that the S_1 population evenly decays to S_0 and T_2, which could explain why approximately one-half of the molecules decay via the fast and the other half via the slow channel. In addition, very similar *cis*-NMTAA quantum yields are predicted for these two channels, since the possible relaxation pathways of the molecule upon reaching the S_0 ground state via an S_1/S_0 conical intersection or via the corresponding T_1/S_0 intersystem crossing are almost identical.

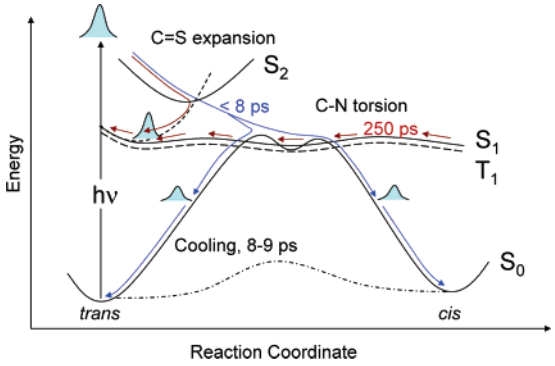

Figure 9. Schematic representation of the photoisomerization reaction of *trans*-NMTAA. The multiple intersections between the S_1, T_1, and the S_0 energy profiles represent the CIs and ISCs documented in Figure 7. See text for details.

5.3. Photoequilibrium and Back-Reaction. Although we could not follow the back-reaction from *cis*- to *trans*-NMTAA with time-resolved spectroscopy, we can deduce from the low cis concentrations at photo equilibrium that cis → trans isomerization must be much more efficient than the trans → cis process. The most reliable ratio of cis → trans over trans → cis isomerization efficiency was determined for 256-nm irradiation, where cis → trans isomerization is 2.3−3.1 times more likely. At the lower error limit of these measurements the sum of both quantum efficiencies may add up to unity. If confirmed by complementary measurements, this could indicate that isomerization proceeds in both directions via a common intermediate state, which then determines the outcome of the photoreaction. This is consistent with a scenario, where the same "region" of the S_1 or T_1 states are populated from either the trans or cis conformers. In other words, in agreement with the proposed mechanism, the decay channels would always correspond to the same set of crossings.

6. Conclusions

Time-resolved infrared experiments and ab initio CASPT2//CASSCF reaction path computations for $\pi-\pi^*$ excitation of *trans*-NMTAA yield consistent mechanistic information on the trans → cis isomerization of NMTAA, which is summarized in Figure 9. The initial S_2 population (schematically represented by a Gaussian wave packet) evolves on S_2 mainly via C−S

(48) Larson, D. B.; Arnett, J. F.; Seliskar, C. J.; McGlynn, S. P. *J. Am. Chem. Soc.* **1974**, *96*, 3370.

bond expansion (and out-of-plane deformation) leading to efficient $S_2 \rightarrow S_1$ decay in the region of the S_2/S_1 conical intersection.

Relaxation on S_1 delivers the system to a very flat region of the potential energy surface, characterized by multiple conformers and multiple S_1/S_0 conical intersections located a few kcal mol^{-1} above them. Decay to the ground state may then occur *directly* (blue arrows) via the S_1/S_0 CIs or *indirectly* (orange arrows). Approximately half of the excited molecules seem to follow the direct relaxation pathway and return to the electronic ground state with a time constant of less than 7 ps. The second half of the excited molecules become temporarily trapped in an electronically excited state and reach the electronic ground state with a much longer time constant of ~250 ps. This population trapping can be the result of either competition between vibrational energy relaxation on S_1 and $S_1 \rightarrow S_0$ electronic decay or competition between fast $S_1 \rightarrow S_0$ decay and a somehow slower relaxation process via the triplet states. On both the fast and the slow time scale, *cis*-NMTAA is formed with a quantum efficiency of 30−40%. We have demonstrated that the final ground-state conformation of NMTAA is predetermined by the molecular geometries of the S_1/S_0 CIs and T_1/S_0 ISCs and is therefore independent of the followed route, provided nearly full sampling of the torsional coordinate in S_1 and/or T_1 is possible prior to decay.

The replacement of one oxygen atom by sulfur in the backbone of a peptide is probably the least "invasive" way to render it photoswitchable. Our study indicates a thio-photoswitch is photostable and potentially capable of inducing conformational change with a high quantum yield on a subnanosecond time scale. This time scale is much faster than the time resolution needed to investigate, for example, the formation of secondary structure elements in proteins. However, notice that, due to the flatness of the S_1 and T_1 isomerization paths, it is likely that a fully relaxed peptide conformation will not be sufficiently perturbed by the photoexcitation of a NMTAA unit. In other words, the S_1 or T_1 force field of NMTAA may not be able to efficiently force a peptide chain out of its equilibrium conformation. On the other hand, if the peptide is exerting a certain amount of torsional strain on the NMTAA unit which is contrasted by the thioamide C−N partial double bond, then promotion to the flat S_1 or T_1 energy surfaces can act as an "unlocking event" (compare the S_0 energy profile with the S_1 and T_1 energy profiles in Figure 7) and allow for trans to cis isomerization. In this case NMTAA may be seen as a photoreleasable lock.

Acknowledgment. We are indebted to Prof. D. Seebach at the ETH in Zürich, who drew our attention to the potential of using thioamides in the investigation of peptide dynamics. Many thanks go to Simon Jurt and Nadja Walch from the NMR service team of the University of Zürich for their quick and competent help. Partial funding has been provided by the Università degli Studi di Siena (Progetto di Ateneo 02/04) and HFSP (RG 0229/2000-M) and the Swiss National Science Foundation (contract 2100-067573.02). We also thank CINECA for granting calculation time.

Supporting Information Available: CASSCF/6-31G* absolute, CASPT2/6-31G* absolute and relative energies along with wave function reference weights and Cartesian coordinates of all structures discussed in the text; calculated and estimated absorption wavelength of the minima along S_1 and T_1 Paths A and B. This material is available free of charge via the Internet at http://pubs.acs.org.

JA049227A